Time-dependent approach to electron pumping in open quantum systems

G. Stefanucci,[1,2,*] S. Kurth,[1,2] A. Rubio,[2,3] and E. K. U. Gross[1,2]

[1]*Institut für Theoretische Physik, Freie Universität Berlin, Arnimallee 14, D-14195 Berlin, Germany*

[2]*European Theoretical Spectroscopy Facility (ETSF), Departamento de Física de Materiales, Universidad del País Vasco, Edificio Korta, 20018 San Sebastian, Spain*

[3]*Departamento de Física de Materiales, Facultad de Ciencias Químicas, UPV/EHU, Unidad de Materiales Centro Mixto CSIC-UPV/EHU and Donostia International Physics Center (DIPC), San Sebastián, Spain*

(Received 12 January 2007; revised manuscript received 2 July 2007; published 29 February 2008)

We use a recently proposed time-dependent approach to investigate the motion of electrons in quantum pump device configurations. The occupied one-particle states are propagated in real time and employed to calculate the local electron density and current. The approach can also be embedded in the framework of time-dependent density functional theory to include electron-electron interactions. An advantage of the present computational scheme is that the same computational effort is required to simulate monochromatic, polychromatic, and nonperiodic drivings. Furthermore, initial-state dependence and history effects are naturally accounted for. We present results for one-dimensional devices exposed to a traveling potential wave. (i) We show that for pumping across a single potential barrier, electrons are transported in pockets and the transport mechanism resembles pumping of water with the Archimedean screw; (ii) we propose a simple model to study pumping through semiconductor nanostructures and we address the phenomenon of the current flowing in the opposite direction to the field propagation; (iii) we present the first numerical evidence of long-lived superimposed oscillations as induced by the presence of bound states and discuss the dependence of their lifetime on the frequency and amplitude of the driving field. By combining Floquet theory with nonequilibrium Green's functions, we also obtain a general expression for the pumped current in terms of inelastic transmission probabilities. This latter result is used for benchmarking our propagation scheme in the long-time limit. Finally, we discuss the limitations of Floquet-based algorithms and suggest our approach as a possible way to go beyond them.

DOI: 10.1103/PhysRevB.77.075339 PACS number(s): 73.23.−b, 05.60.Gg, 72.10.−d, 73.63.−b

I. INTRODUCTION

The continuous progress in manipulating single molecules chemically bound to macroscopic reservoirs has led to the emerging field of molecular electronics.[1] Besides the widely studied stationary case, today experimental techniques enable the study of time-dependent phenomena in open quantum systems, such as photon-assisted transport and electron pumping through real or artificial molecules.

An electron pump is an electronic device generating a net current between two unbiased electrodes. Pumping is typically achieved by applying a periodic gate voltage depending on two or more parameters.[2–4] Electron pumps have been realized experimentally, e.g., for an open semiconductor quantum dot[5] driven by two harmonic gate voltages with a phase shift, and for an open nanotube[6] driven by an electrostatic potential wave. Recently, monoparametric pumping devices have also been realized[7,8] and studied theoretically, see the works of Wang *et al.*,[9] Vavilov *et al.*,[8] and Foa Torres.[10]

In the literature, different techniques have been used to discuss electron pumping theoretically. For slowly varying electric fields,[11] the device remains in equilibrium and the pumping process is adiabatic.[5,12] To describe adiabatic pumpings, Brouwer[4] has suggested a framework based on the scattering approach of Büttiker *et al.*[13,14] An alternative and equivalent formulation based on Keldysh-Green's function theory has been proposed by Zhou *et al.*[15] A natural way to go beyond the adiabatic case is to apply Floquet theory. Within an equation-of-motion approach Camalet *et al.*[16] have found a general expression for the average total current and for the noise power of electrons pumped in a tight-binding wire. Alternatively, one can combine Floquet theory with nonequilibrium Green's function techniques.[3,17,18] Generally speaking, Floquet-based approaches provide a very powerful tool to calculate average quantities of periodically driven systems. However, going beyond the monochromatic case quite quickly becomes computationally demanding. Furthermore, such approaches are not applicable to the study of transient effects and nonperiodic phenomena.

In this work, we use a recently proposed time-dependent approach,[19] which is well suited to study the effects of an electric field, such as a gate voltage or a laser field, on the electron dynamics of a nanoscale junction. We show the feasibility of our numerical scheme by calculating the full time dependence (including the transient behavior) of observables such as the local density and current. The method is designed to deal with arbitrary frequencies and the same computational effort is required for both monochromatic and polychromatic drivings as well as for nonperiodic perturbations. We consider three different quantum pump configurations driven by an electrostatic potential wave. For the case of a single barrier, we show that the density is transported in pockets (density maxima at potential minima), a phenomenon that resembles pumping of water with the Archimedean screw. The possibility of describing transport at the nanoscale using a hydrodynamic approach has been put forward in Ref. 20 and our time-dependent simulation provides an explicit example of essentially classical fluid dynamics (in the case of a purely kinetic stress tensor) as obtained from the

quantum laws of motion. Second, we study pumping through semiconductor nanostructures as, e.g., carbon nanotubes.[6] We propose to model the device by a series of one-dimensional potential barriers and we show that, despite the simplicity of the model, the pumped current versus Fermi energy has the same qualitative behavior as the pumped current measured by Leek *et al.*[6] We also address the phenomenon of current inversion, i.e., the direction of the particle current being opposite to the direction of the field propagation. We provide an explanation based on inelastic scatterings and corroborate the picture with a real-time simulation. The quantum mechanism of absorption and/or emission of quanta of the driving field is shown to correspond to "bubbles" (in the electron liquid) moving in the same direction of the traveling wave, and hence an excess of density moving in the opposite direction. In the last example, we investigate transient regimes, a topic which is gaining increasing attention in the quantum transport community.[19,21–30] We specialize to quantum wells and provide the first numerical evidence of long-lived superimposed oscillations as induced by the presence of bound states. In the limit of weak driving fields, we also discuss the dependence of their lifetime on the frequency and amplitude of the perturbing field.

The paper is organized as follows. In Sec. II, we describe the system consisting of two macroscopic reservoirs connected to a central device. We combine the Floquet theory with the Keldysh formalism to study the long-time behavior of the device, and we generalize the formula for the average current by Camalet *et al.*[16] Some general features of Floquet-based algorithms are discussed. To overcome the limitations of the Floquet theory, we use a recently proposed real-time approach based on the propagation of the occupied single-particle states.[19] Full implementation details are given for one-dimensional electrodes and arbitrary device geometries. A detailed comparison between the numerical performance of Floquet-based schemes and our method is also made. In Sec. III, we show our numerical results which demonstrate that the real-time propagation offers an alternative route to investigate open quantum systems and provides a complementary picture of the microscopic dynamics. In Sec. IV, we summarize the main results and discuss future projects.

II. TIME-DEPENDENT CURRENT

We consider an open quantum system C (central region) connected to two macroscopically large reservoirs L and R (left and right electrodes). We are interested in describing the electron dynamics when region C is disturbed by arbitrary time-dependent electric fields. Assuming that the reservoirs are not directly connected, the one-particle Hamiltonian of the entire system reads

$$\mathbf{H}(t) = \begin{bmatrix} \mathbf{H}_{LL} & \mathbf{H}_{LC} & 0 \\ \mathbf{H}_{CL} & \mathbf{H}_{CC}(t) & \mathbf{H}_{CR} \\ 0 & \mathbf{H}_{RC} & \mathbf{H}_{RR} \end{bmatrix}. \tag{1}$$

The Hamiltonian $\mathbf{H}_{\alpha\alpha}$, $\alpha=L,R$, as well as the Hamiltonian of the central region $\mathbf{H}_{CC}$ are obtained by projecting the full Hamiltonian $\mathbf{H}$ onto the subspace of the corresponding region. How to choose the one-particle states in regions L, R, or C depends on the specific problem at hand. We can use, e.g., a real-space grid for *ab initio* calculations, or a tight-binding representation for model calculations, or even different basis functions for different regions (for instance, eigenfunctions of the reservoirs for L and R, and localized states for C).[31] The off-diagonal parts in Eq. (1) account for the contacts and are given in terms of matrix elements of $\mathbf{H}$ between states of C and states of L and R. We use atomic units throughout the paper.

In many applications of physical interest, the driving field is periodic in time. In this case, it is possible to work out an analytic expression for the dc component of the total current I_{dc}, provided memory effects and initial-state dependence are washed out in the long-time limit. Below, we combine the Floquet formalism with nonequilibrium Green's functions and generalize the formula for I_{dc} by Camalet *et al.*[16] to arbitrary contacts. We also discuss the limitations of Floquet theory and propose an alternative approach based on the real-time propagation of the initially occupied states of the system.

A. Long-time limit: Floquet theory and Keldysh formalism

Most approaches to driven nanoscale systems are based on a fictitious partitioning first introduced by Caroli *et al.*[32] The initial many-particle state is a Slater determinant of eigenstates of the *isolated* left and right reservoirs with eigenenergy below some chemical potential μ. A more physical initial state has been considered by Cini.[33] It is a Slater determinant of eigenstates of the *contacted* system $L+C+R$ with eigenenergy smaller than μ. Independent of the initial state, it has been proved[21,34] that the number of electrons per unit time that leave the $\alpha=L,R$ reservoir is given by the formula[35]

$$I_\alpha(t) = 2\ \mathrm{Re}\ \mathrm{Tr}[\mathbf{Q}_\alpha(t)], \tag{2}$$

$$\mathbf{Q}_\alpha(t) = \{\mathbf{G}^R \cdot \mathbf{\Sigma}_\alpha^< + \mathbf{G}^R \cdot \mathbf{\Sigma}^< \cdot \mathbf{G}^A \cdot \mathbf{\Sigma}_\alpha^A\}(t;t), \tag{3}$$

provided that (a) t goes to infinity and (b) the retarded Green's function projected on the central region $\mathbf{G}^R$ (or the advanced one $\mathbf{G}^A$) vanishes when the separation between its time arguments goes to infinity. In the above equation, $\mathbf{\Sigma}=\mathbf{\Sigma}_L+\mathbf{\Sigma}_R$ is the embedding self-energy in the long-time limit and the symbol Tr denotes a trace over a complete set of states of the central region. We also have used the short-hand notation $\{f\cdot g\}(t_1;t_2) \equiv \int_{-\infty}^{\infty} d\bar{t} f(t_1;\bar{t}) g(\bar{t};t_2)$ for the convolution of two functions f and g.

For an applied bias U_α in reservoir $\alpha=L,R$, which is constant in time, the embedding self-energy depends only on the difference between its time arguments. Let

$$\mathbf{\Sigma}_\alpha^{R/A}(\omega) = \mathbf{\Lambda}_\alpha(\omega) \mp \frac{i}{2}\mathbf{\Gamma}_\alpha(\omega) \tag{4}$$

be the Fourier transform of the retarded/advanced self-energy. The imaginary part $\mathbf{\Gamma}_\alpha$ is the contribution of region α to the local spectral density. The Fourier transform of the lesser self-energy is then given by

$$\mathbf{\Sigma}_\alpha^<(\omega) = i f_\alpha(\omega)\mathbf{\Gamma}_\alpha(\omega), \tag{5}$$

where $f_\alpha(\omega)=f(\omega-U_\alpha)$ is the Fermi distribution function.

Let us specialize to periodic time-dependent perturbations in region C: $\mathbf{H}_{CC}(t)=\mathbf{H}_{CC}(t+T_0)$. According to Floquet theory, we assume that the Green's function in Eq. (3) can be expanded as follows:

$$\mathbf{G}^{R/A}(t;t') = \sum_m \int \frac{d\omega}{2\pi}\mathbf{G}_m^{R/A}(\omega)e^{-i\omega(t-t')+im\omega_0 t'}, \tag{6}$$

where $\omega_0=2\pi/T_0$ is the frequency of the driving field. We wish to emphasize that the above expansion is justified only if all observable quantities (calculable from $\mathbf{G}$) oscillate in time with the same frequency as the external field (we thus exclude those cases where the initial-state dependence and/or history dependence are not washed out in the long-time limit). This is typically the case for adiabatic switchings (for a detailed discussion on the existence of the adiabatic limit in Floquet theory, see Ref. 36).

Inserting Eq. (6) into Eq. (3) and extracting the dc component, we obtain

$$\mathbf{Q}_{\alpha,\mathrm{dc}} \equiv \lim_{t\to\infty}\frac{1}{T_0}\int_t^{t+T_0} d\bar{t}\mathbf{Q}_\alpha(\bar{t}) = \int \frac{d\omega}{2\pi}\mathbf{G}_0(\omega)\mathbf{\Sigma}_\alpha^<(\omega) + \int \frac{d\omega}{2\pi}\sum_m \mathbf{G}_m(\omega)\mathbf{\Sigma}^<(\omega)\mathbf{G}_m^\dagger(\omega)\mathbf{\Sigma}_\alpha^A(\omega-m\omega_0), \tag{7}$$

where we have defined

$$\mathbf{G}_m(\omega) \equiv \mathbf{G}_m^R(\omega-m\omega_0) = [\mathbf{G}_{-m}^A(\omega)]^\dagger. \tag{8}$$

The last equality in Eq. (8) follows directly from the identity $\mathbf{G}^R(t;t')=[\mathbf{G}^A(t';t)]^\dagger$. The dc component $I_{\alpha,\mathrm{dc}}$ of the time-dependent total current $I_\alpha(t)$ is given by the right hand side of Eq. (2) with $\mathbf{Q}_\alpha(t)$ replaced by $\mathbf{Q}_{\alpha,\mathrm{dc}}$. In the Appendix, we show that in the monochromatic case,

$$\mathbf{H}_{CC}(t) = \mathbf{H}_{CC}^0 + \mathbf{U}_+ e^{i\omega_0 t} + \mathbf{U}_- e^{-i\omega_0 t}, \tag{9}$$

the resulting expression for $I_{\alpha,\mathrm{dc}}$ can be cast in a Landauer-like formula

$$I_{L,\mathrm{dc}} = \sum_m \int \frac{d\omega}{2\pi}[f_L(\omega)T_{m,L}(\omega) - f_R(\omega)T_{m,R}(\omega)], \tag{10}$$

and $I_{R,\mathrm{dc}}=-I_{L,\mathrm{dc}}$, as it should be due to charge conservation. The "inelastic" transmission coefficients $T_{m,\alpha}$ may be interpreted as the probability for electrons to be transmitted from one reservoir to the other with the absorption or emission of m quanta of the driving field. They can be written as

$$T_{m,L}(\omega) = \mathrm{Tr}[\mathbf{\Gamma}_L(\omega)\mathbf{G}_m^\dagger(\omega)\mathbf{\Gamma}_R(\omega-m\omega_0)\mathbf{G}_m(\omega)], \tag{11}$$

$$T_{m,R}(\omega) = \mathrm{Tr}[\mathbf{\Gamma}_R(\omega)\mathbf{G}_m^\dagger(\omega)\mathbf{\Gamma}_L(\omega-m\omega_0)\mathbf{G}_m(\omega)]. \tag{12}$$

The above equations resemble the trace formula obtained by Meir and Wingreen in the case of a static bias.[37]

We observe that for zero driving the Fourier coefficients $\mathbf{G}_m$, and hence the transmission probabilities $T_{m,\alpha}$, are all zero except for $m=0$, and Eq. (10) reduces to the well-known Landauer formula for steady-state currents.[38] On the contrary, all the $T_{m,\alpha}$'s contribute to the average current when a driving field is present. The corresponding $\mathbf{G}_m$'s can be computed recursively from the zeroth order coefficient $\mathbf{G}_0$, as it has been shown in Ref. 39 (see also the Appendix). It is also worth emphasizing that our formula for the $T_{m,\alpha}$'s correctly reduces to the one of Camalet *et al.*[16] for a central region described by a tight-binding wire of sites $|1\rangle,\ldots,|N\rangle$ and connected to the left reservoir through $|1\rangle$ and to the right reservoir through $|N\rangle$. In this case, the spectral density matrices $\mathbf{\Gamma}_\alpha$ have only one nonvanishing entry, $[\mathbf{\Gamma}_L]_{n,m}=\delta_{n,1}\delta_{m,1}\gamma_L$ and $[\mathbf{\Gamma}_R]_{n,m}=\delta_{n,N}\delta_{m,N}\gamma_R$, and the coefficients $T_{m,\alpha}$ can be rewritten as

$$T_{m,L}(\omega) = \gamma_L(\omega)\gamma_R(\omega-m\omega_0)|[\mathbf{G}_m(\omega)]_{N,1}|^2, \tag{13}$$

$$T_{m,R}(\omega) = \gamma_R(\omega)\gamma_L(\omega-m\omega_0)|[\mathbf{G}_m(\omega)]_{1,N}|^2. \tag{14}$$

Equation (10) demonstrates how the initial Floquet assumption of Eq. (6) allows for carrying the analytic calculation of the current [Eq. (2)] much further and eventually delivers a simple numerical scheme for the computation of the average current. Despite the enormous success in predicting ac dynamical properties of many different nanoscale conductors, Floquet theory might be inadequate to face the future challenges of nanotechnology.[40] Below, we discuss some limitations of Floquet-based approaches.

(i) *Numerical performance*. For later comparison with our proposed real-time approach, we briefly report on the numerical performance of Floquet algorithms, such as the recursive scheme described in the Appendix. Let N be the number of basis functions in region C. For a given frequency ω, the calculation of $\mathbf{G}_0(\omega)$ requires the inversion of $m_{\max}$ complex matrices of dimension $N\times N$. The number $m_{\max}$ should be chosen such that the cutoff energy $E_{\max}=m_{\max}\omega_0$ is much larger than any other energy scale in the problem. Typically, $m_{\max}$ is in the range from 10 to 100. The coefficients $\mathbf{G}_{\pm m}(\omega)$, $m>0$, are then calculated from $\mathbf{G}_{\pm(m-1)}(\omega)$ by simple matrix multiplications according to Eq. (A20). Knowing the $\mathbf{G}_m$'s, one can compute the inelastic transmission probabilities from Eqs. (11) and (12), and hence the average current.

In the above procedure, most of the computational time is spent for matrix inversions and matrix multiplications. We can roughly estimate the overall time of a full run as $T_{\mathrm{run}} \simeq m_{\max}\times N_\omega\times(\tau_i+\tau_m)$, where N_ω is the number of mesh points (generally not uniform) along the ω axis used to evaluate the integral in Eq. (10), and τ_i (τ_m) is the time for a single matrix inversion (multiplication). In our case, both τ_i and τ_m scale as N^3. Depending on the system and on the external driving forces, the inelastic transmission probabilities might exhibit quite sharp peaks as function of energy. Therefore, for an accurate computation of the energy integral in Eq. (10), a fine energy grid is required, which means that N_ω is large. In the numerical calculations of Sec. III, N_ω is in the range of 100–1000. We conclude that $T_{\mathrm{run}}/(\tau_i+\tau_m) \sim 10^3$–$10^5$.

(ii) *Periodic potentials*. Beyond the monochromatic case,

the recursive scheme of the Appendix becomes computationally demanding. The inclusion of one, two, etc., more harmonics in the expansion of the driving field [see Eq. (A4)] transforms the block tridiagonal system of equations for the $\mathbf{G}_m$'s into a block pentadiagonal, heptadiagonal, etc., system of equations. For arbitrary periodic drivings, a Floquet-based approach may not be feasible.

(iii) *Arbitrary time-dependent potentials*. Besides the wide class of periodic drivings, it is of interest to investigate the response of a nanodevice to nonperiodic drivings as well.[41] In such cases, the Floquet formalism does not apply and a full time-dependent approach is required.

(iv) *Transients*. The Landauer formalism provides a very powerful technique to calculate nonequilibrium quantities in steady-state regimes. Similarly, the Floquet formalism allows to calculate nonequilibrium quantities in "oscillating-state" regimes, i.e., when all transient effects are died off. However, transient responses can be expected to become of some relevance in the future. Molecular devices will eventually be integrated in nanoscale circuits and respond to ultrafast external signals. Transient effects in such operative regimes may not be irrelevant, as it has been recently recognized by several authors.[19,21–30] In Sec. III, we provide explicit evidence of long-lived superimposed oscillations in the time-dependent current profile. The frequencies of these oscillations are not commensurable with the driving frequency, and have to be ascribed to the presence of "adiabatic" bound states.[42,43]

B. Real-time propagation

In this section, we propose an alternative approach to driven nanoscale transport. The main idea is to calculate the time-dependent total current from the time-dependent wave functions $|\psi_s(t)\rangle$, where $|\psi_s(0)\rangle$ is the sth eigenstate of the system $L+C+R$ before the time-dependent perturbation is switched on. Our approach does not rely on the Floquet assumption, and is free from *all* the limitations discussed previously. Furthermore, the computational time is comparable with Floquet-based algorithms.

As the full Hamiltonian $\mathbf{H}(t)$ refers to an extended and nonperiodic system, we cannot solve *brute force* the Schrödinger equation[44]

$$i\frac{d}{dt}|\psi(t)\rangle = \mathbf{H}(t)|\psi(t)\rangle. \tag{15}$$

Fortunately, we do not need to calculate the time-dependent wave function everywhere in the system in order to calculate the total current. The knowledge of the wave function in region C is enough for our purposes (see below). Denoting with $|\psi_C(t)\rangle$, the wave function projected on region C and with $|\psi_\alpha(t)\rangle$ the wave function projected on region $\alpha=L, R$, it is straightforward to show that Eq. (15) implies the following equation for $|\psi_C(t)\rangle$:[45]

$$i\frac{d}{dt}|\psi_C(t)\rangle = \mathbf{H}_{CC}(t)|\psi_C(t)\rangle + \int_0^t \mathbf{\Sigma}^R(t;t')|\psi_C(t')\rangle + \sum_{\alpha=L,R} \mathbf{H}_{C\alpha}\exp(-i\mathbf{H}_{\alpha\alpha}t)|\psi_\alpha(0)\rangle, \tag{16}$$

where

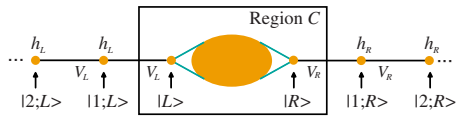

FIG. 1. (Color online) The schematic sketch of the electrode-junction-electrode system with semiperiodic one-dimensional electrodes.

$$\mathbf{\Sigma}^R(t;t') = \sum_{\alpha=L,R} \mathbf{H}_{C\alpha}\exp[-i\mathbf{H}_{\alpha\alpha}(t-t')]\mathbf{H}_{\alpha C} \tag{17}$$

is the Fourier transform of the embedding self-energy in Eq. (4).

Equation (16) is an *exact* equation for the time evolution of open systems, but is still not suited for a numerical implementation. The importance of charge conservation in quantum transport makes the unitary property a fundamental requirement. In this work, we use a unitary algorithm which has been recently proposed to study electron transport in biased electrode-device-electrode systems.[19] Below, we illustrate the main ideas and specialize the formulas of Ref. 19 to one-dimensional reservoirs.

For a given initial state $|\psi(0)\rangle=|\psi^{(0)}\rangle$, we calculate the time-evolved state $|\psi(t_m=2m\delta)\rangle=|\psi^{(m)}\rangle$ by approximating Eq. (15) with the Crank-Nicholson formula

$$(\mathbf{1}+i\delta\mathbf{H}^{(m)})|\psi^{(m+1)}\rangle = (\mathbf{1}-i\delta\mathbf{H}^{(m)})|\psi^{(m)}\rangle, \tag{18}$$

with $\mathbf{H}^{(m)}=\frac{1}{2}[\mathbf{H}(t_{m+1})+\mathbf{H}(t_m)]$. The above propagation scheme is unitary (norm conserving) and accurate to second order in δ. From Eq. (18), we can extract an equation for the time-evolved state in region C, similar to what we have done for the derivation of Eq. (16). The final result is

$$(\mathbf{1}_C+i\delta\mathbf{H}^{(m)}_{\text{eff}})|\psi_C^{(m+1)}\rangle = (\mathbf{1}_C-i\delta\mathbf{H}^{(m)}_{\text{eff}})|\psi_C^{(m)}\rangle + |S^{(m)}\rangle - |M^{(m)}\rangle, \tag{19}$$

with $\mathbf{1}_C$ the identity matrix in region C. Equation (19) is the proper (unitary) time discretization of Eq. (16). Moreover, Eq. (19) is ready to be implemented since it contains only *finite-size* matrices and vectors (with the dimension used to describe the central region as, e.g., the number of lattice sites in a tight-binding representation or the number of grid points in a real-space grid representation). In the following, we give full implementation details of the *memory term* $|M^{(m)}\rangle$, the *source term* $|S^{(m)}\rangle$, and the *effective Hamiltonian* $\mathbf{H}^{(m)}_{\text{eff}}$ appearing in Eq. (19).

For the sake of simplicity, we consider one-dimensional semi-infinite reservoirs described by tridiagonal matrices $\mathbf{H}_{\alpha\alpha}$, $\alpha=L, R$, with diagonal entries h_α and off-diagonal entries V_α, see Fig. 1. For tight-binding models, the parameter h_α represents the on-site energy while the parameter V_α represents the hopping integral between nearest-neighbor sites. The Hamiltonian $\mathbf{H}_{\alpha\alpha}$ is also suited to describe continuum models with a three-point discretization of the kinetic term. In this case, the parameter $h_\alpha=1/\Delta x^2+U_\alpha$ and $V_\alpha=-1/(2\Delta x^2)$, where Δx is the grid spacing. We would like to

emphasize that the algorithm can easily be generalized to reservoirs with an arbitrary semi-infinite periodicity and it is not limited to one-dimensional systems.[19]

Without loss of generality, we consider a central region that includes few sites of the left and right reservoirs, and we denote by $|\alpha\rangle$ the state where only the site of region C connected to the reservoir $\alpha=L, R$ is occupied (see Fig. 1).

The *memory state* $|M^{(m)}\rangle$ stems from the second term on the r.h.s. of Eq. (16) and reads

$$|M^{(0)}\rangle = 0, \tag{20}$$

while for $m \geqslant 1$, we have

$$|M^{(m)}\rangle = \delta^2 \sum_{\alpha=L,R} |\alpha\rangle \sum_{k=0}^{m-1} [\langle\alpha|\psi_C^{(k+1)}\rangle + \langle\alpha|\psi_C^{(k)}\rangle] \times [q_\alpha^{(m-k)} + q_\alpha^{(m-k-1)}]. \tag{21}$$

The q coefficients can be computed recursively according to

$$q_\alpha^{(0)} = \frac{-(1+i\delta h_\alpha) + \sqrt{(1+i\delta h_\alpha)^2 + (2\delta V_\alpha)^2}}{2\delta^2}, \tag{22}$$

$$q_\alpha^{(1)} = \frac{1 - i\delta h_\alpha - 2\delta^2 q_\alpha^{(0)}}{1 + i\delta h_\alpha + 2\delta^2 q_\alpha^{(0)}} q_\alpha^{(0)}, \tag{23}$$

and for $m \geqslant 2$

$$q_\alpha^{(m)} = \frac{q_\alpha^{(1)} q_\alpha^{(m-1)}}{q_\alpha^{(0)}} - \delta^2 \frac{q_\alpha^{(0)} q_\alpha^{(m-2)}}{1 + i\delta h_\alpha + 2\delta^2 q_\alpha^{(0)}} - \delta^2 \sum_{k=1}^{m-1} \frac{q_\alpha^{(k)} + 2q_\alpha^{(k-1)} + q_\alpha^{(k-2)}}{1 + i\delta h_\alpha + 2\delta^2 q_\alpha^{(0)}} q_\alpha^{(m-k)}, \tag{24}$$

with the convention that $q_\alpha^{(m)}=0$ for negative m.

The *source state* $|S^{(m)}\rangle$ stems from the last term on the r.h.s. of Eq. (16) and reads

$$|S^{(m)}\rangle = -2i\delta \sum_{\alpha=L,R} \mathbf{H}_{C\alpha} \frac{(\mathbf{1}_\alpha - i\delta \mathbf{H}_{\alpha\alpha})^m}{(\mathbf{1}_\alpha + i\delta \mathbf{H}_{\alpha\alpha})^{m+1}} |\psi_\alpha(0)\rangle, \tag{25}$$

where $\mathbf{1}_\alpha$ is the unit matrix in region α. The source state depends on the initial wave function in the reservoirs. As we are interested in propagating eigenstates of $\mathbf{H}(0)$, $|\psi_\alpha(0)\rangle$ has the following general expression:

$$|\psi_\alpha^{(0)}\rangle = A_\alpha^{(+)} |+p_\alpha\rangle + A_\alpha^{(-)} |-p_\alpha\rangle, \tag{26}$$

with

$$|p_\alpha\rangle = \sum_{j=1}^{\infty} e^{ip_\alpha j} |j;\alpha\rangle, \tag{27}$$

and the state $|j;\alpha\rangle$, where only the jth site of reservoir $\alpha=L, R$ is occupied, see Fig. 1. For extended states in region α the parameter p_α is real. For bound states or fully reflected states in region α, the parameter p_α is imaginary and the amplitude $[A_\alpha^{(+)}$ or $A_\alpha^{(-)}]$ of the growing exponential is zero. No matter if p_α is real or imaginary, one can prove that

$$\mathbf{H}_{C\alpha} \frac{(\mathbf{1}_\alpha - i\delta \mathbf{H}_{\alpha\alpha})^m}{(\mathbf{1}_\alpha + i\delta \mathbf{H}_{\alpha\alpha})^{m+1}} |p_\alpha\rangle = \zeta_\alpha^{(m)} |\alpha\rangle, \tag{28}$$

with

$$\zeta_\alpha^{(m)} = e^{ip_\alpha} V_\alpha \gamma_\alpha^{(m)} + i\delta \sum_{k=0}^{m} \gamma_\alpha^{(m-k)} [q_\alpha^{(k)} + q_\alpha^{(k-1)}], \tag{29}$$

and

$$\gamma_\alpha^{(m)} = \frac{(1 - i\delta h_\alpha - 2i\delta V_\alpha \cos p_\alpha)^m}{(1 + i\delta h_\alpha + 2i\delta V_\alpha \cos p_\alpha)^{m+1}}. \tag{30}$$

Finally, the *effective Hamiltonian* is given by

$$\mathbf{H}_{\text{eff}}^{(m)} = \mathbf{H}_{CC}^{(m)} - i\delta \sum_{\alpha=L,R} q_\alpha^{(0)} |\alpha\rangle\langle\alpha|. \tag{31}$$

The above algorithm allows us to calculate the time evolution of *any* initial state whose wave function in the reservoirs has the form in Eq. (26). This is the case of both the contacting approach by Caroli *et al.* and the partition-free approach by Cini. In the former approach, the initial one-particle states are eigenstates of the isolated left and right reservoirs, meaning that

$$|\psi_\alpha^{(0)}\rangle = 2\sum_{j=1}^{\infty} \sin(p_\alpha j) |j;\alpha\rangle = \frac{|+p_\alpha\rangle - |-p_\alpha\rangle}{i}, \tag{32}$$

for $\alpha=L$ (or $\alpha=R$), zero for $\alpha=R$ (or $\alpha=L$), and zero in region C. In the latter approach, the computation of the initial one-particle states is more involved. Here, we have used a recently proposed general scheme based on the diagonalization of the imaginary part of the retarded Green's function.[19] This scheme may also be used for arbitrary, semi-periodic electrodes. In the special case of spatially uniform one-dimensional reservoirs, one can, of course, always use the textbook procedure of matching the wave function at the interfaces.

Denoting with $|\psi_{s,C}(t)\rangle$, the evolution of the original eigenstate $|\psi_s(0)\rangle$ in the central region, we can calculate the time-dependent occupation $\rho(j,t)$ of a state $|j\rangle$ in region C according to

$$\rho(j,t) = \sum_s f(\varepsilon_s) |\langle j|\psi_{s,C}(t)\rangle|^2, \tag{33}$$

where ε_s is the eigenvalue of $\mathbf{H}(0)$ corresponding to the eigenvector $|\psi_s(0)\rangle$ and $f(\varepsilon)$ is the Fermi distribution function. Similarly, the total time-dependent current $I_\alpha(t)$ can be calculated from the time derivative of the total number of particles in electrode α and reads

$$I_\alpha(t) = -2\sum_s f(\varepsilon_s) \sum_{j\neq\alpha} \text{Im}\langle j|\psi_{s,C}(t)\rangle\langle\psi_{s,C}(t)|\alpha\rangle [\mathbf{H}_{CC}(t)]_{\alpha j}, \tag{34}$$

where the sum is over all states j of region C except the state $|\alpha\rangle$. We observe that for systems out of steady-state regimes $I_L(t)+I_R(t)=I_d(t)\neq 0$, where

$$I_d(t) = \frac{d}{dt} \sum_{j \neq L,R} \rho(j,t) \tag{35}$$

is the displacement current.

We wish to conclude this section with a discussion on the performance of our method and a comparison with Floquet-based approaches.

(i) The computational time $T_{\rm run}$ scales linearly with the number of states N_s used to evaluate the sum in Eq. (33) or Eq. (34), and quadratically with the number of time steps N_t. In most cases, transient effects disappear after few femtoseconds (few tens of a.u.). Using a time step of the order of 10^{-2} a.u., we can obtain a rather good estimate of $I_{\alpha,\rm dc}$ with $N_t \sim 10^3 - 10^4$. Given a central regions with hundreds of states, the real-time algorithm can be of the same speed of or even faster than the Floquet algorithm of the Appendix.

(ii) The real-time algorithm can deal with arbitrary (periodic and nonperiodic) drivings, and the computational time is independent of the specific time dependence of $\mathbf{H}_{CC}(t)$. Moreover, the algorithm is easily generalized[19] to deal with spatially uniform bias potentials in the electrodes with arbitrary dependence on time, such as for an ac bias.

(iii) From the time-evolved states $|\psi_s(t)\rangle$, we have access to the total current $I_\alpha(t)$ at *any* time t, and not only to the long-time limit of the dc component of $I_\alpha(t)$. In particular, we can easily investigate transients and the full shape of $I_\alpha(t)$ for $t \to \infty$. In practice, this limit is achieved for a finite time $T_{\rm max}$ after which all transient phenomena have died out.

(iv) Another advantage of our method is the possibility of including electron-electron interactions via time-dependent density functional theory.[46] Indeed, the external potential is local in both space and time provided the initial state is the ground state of the contacted system. Therefore, according to the Runge-Gross theorem,[46,47] the interacting time-dependent density can be reproduced in a fictitious system of noninteracting electrons moving under the influence of an effective Kohn-Sham potential which is local in space and time. We observe that this is not the case in the contacting approach since the switching of the contacts makes the external potential nonlocal in space and hence the Runge-Gross theorem does not apply.

(v) Finally, we would like to stress that the Hamiltonian $\mathbf{H}_{CC}(t)$ enters in the algorithm only via the effective Hamiltonian $\mathbf{H}_{\rm eff}$ of Eq. (31), and has no restrictions. Thus, besides one-dimensional structures (like those considered in Sec. III), one can consider other geometries as well, such as those of planar molecules, quantum rings, nanotubes, jellium slabs, etc.

III. NUMERICAL RESULTS

In this section, we illustrate the performance of the proposed scheme by presenting our results for one-dimensional continuous systems described by the time-dependent Hamiltonian,

$$H(x,t) = -\frac{\nabla^2}{2} + U(x,t). \tag{36}$$

We discretize H on an equidistant grid and use a three-point discretization for the kinetic term. Within this model, we study various model systems highlighting different features in electron pumping.

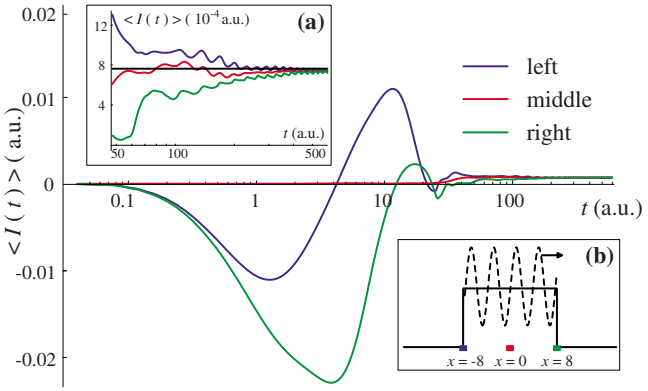

FIG. 2. (Color online) Time-dependent average current at the left [blue (dark gray)] and right [green (light gray)] interfaces and in the middle of region C [red (gray)] for pumping through a single square barrier by a traveling wave. The traveling potential wave is restricted to the propagation window $|x| < 8$ a.u. and has the form $U(x,t) = U_1 \sin(qx - \omega_0 t)$ with amplitude $U_1 = 0.35$ a.u., wave number $q = 1.6$ a.u., and frequency $\omega_0 = 0.2$ a.u. Inset (a) is a magnification of the long-time behavior. The straight line corresponds to the value $I_{L,\rm dc} = 7.63 \times 10^{-4}$ a.u. of the average current calculated using the Floquet algorithm. Inset (b) displays the static potential barrier (solid line) and the superimposed right-moving traveling wave (dashed line).

A. Archimedean screw

As a first example of electron pumping, we have calculated the time evolution of the density and total current for a single square barrier exposed to a traveling potential wave $U(x,t) = U_1 \sin(qx - \omega_0 t)$. The wave is spatially restricted to the explicitly treated device region which in our case also coincides with the static potential barrier. The barrier extends from $x = -8$ a.u. to $x = +8$ a.u. and its height is 0.5 a.u., see inset (b) in Fig. 2. The system is unbiased, i.e., $U_L = U_R = 0$, and the Fermi energy of the initial (ground) state is $\varepsilon_F = 0.3$ a.u. For the numerical implementation, we have chosen a lattice spacing $\Delta x = 0.08$ a.u., and 200 k points between 0 and $k_F = \sqrt{2\varepsilon_F}$ which amounts to the propagation of 400 states.

In Fig. 2, we plot the time-dependent average current calculated according to

$$\langle I(t) \rangle = \theta(T_0 - t) \frac{1}{t} \int_0^t d\tau I(\tau) + \theta(t - T_0) \frac{1}{T_0} \int_{t-T_0}^t d\tau I(\tau), \tag{37}$$

with the period of the traveling wave $T_0 = 2\pi/\omega_0$. For the time propagation, we have chosen a time step $2\delta = 0.02$ a.u. As expected $\langle I(t) \rangle$ converges to some steady value $I_{L,\rm dc}$ after a transient time of the order of 50–60 a.u. We have calculated the average current in three different points of region C and verified that the steady value does not depend on the position. The dc limit $I_{L,\rm dc}$ can also be computed from the

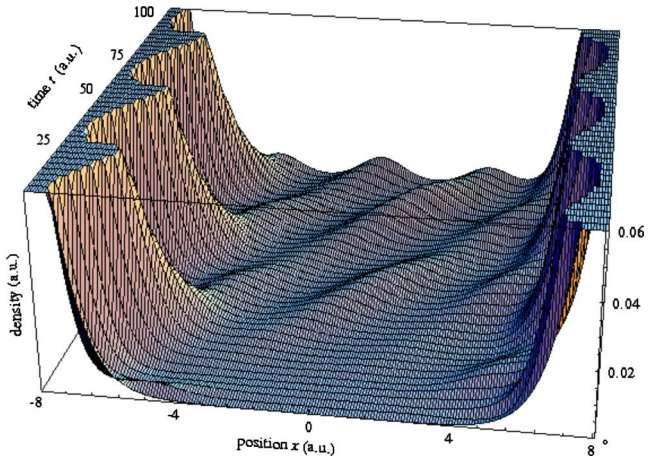

FIG. 3. (Color online) Time-dependent density in region C as a function of position x and time t. The range for $\rho(x,t)$ is between 0 and 0.06 a.u. for improved visibility of the pockets of density. All parameters are the same as for Fig. 2.

Floquet algorithm of the Appendix. Using $m_{\max}=15$ and $N_\omega=150$ energy points between 0 and ε_F, we find $I_{L,\mathrm{dc}}=7.63\cdot10^{-4}$ a.u., in very good agreement with the average current of the time propagated system, see inset (a) of Fig. 2.

In Fig. 3, we plot the time-dependent density $\rho(x,t)$ in the device region as a function of both position x and time t. The density exhibits local maxima in the potential minima and is transported in pockets by the wave. From Fig. 3, it is also evident that the height of the pockets is not uniform over the system, and reaches its maximum around $x=0$. We also notice that the particle current flows in the same direction as the driving wave. The pumping mechanism in this example resembles pumping of water with the Archimedean screw. The observed classical behavior of the electron fluid is in agreement with the predictions of a recent hydrodynamic approach[20] to transport at the nanoscale (in our example the stress tensor is purely kinetic).

B. Pumping through a semiconductor nanostructure

The second example was motivated by a recent experiment on pumping through a carbon nanotube by Leek *et al.*[6] The arrangement has been suggested by Talyanskii *et al.*[48] and is as follows. A semiconducting nanotube lying on a quartz substrate is placed between two metallic contacts. A transducer generates an acoustic wave on the surface of the piezoelectric crystal. The crystal responds by generating an electrostatic potential wave which acts like our traveling wave on the electrons in the nanotube. The direction of the pumping current is found to depend on the applied gate voltage. A pumping current flowing in the direction opposite to the propagation direction of the traveling wave has been interpreted in a stationary picture as a predominant hole tunneling over electron tunneling. To reproduce such an inversion in the current flow, we have modeled the nanotube with a periodic static corrugation $U_0(x)=U_C[1+\cos(kx)]$ in region C, with $U_C=0.5$ a.u. and $k=10\pi/6\sim5.2$ a.u. (see inset in Fig. 4). For a traveling wave $U(x,t)=U_1\sin(qx-\omega_0 t)$, with

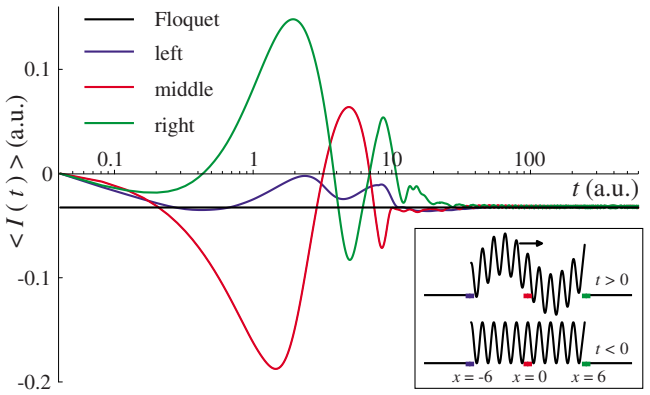

FIG. 4. (Color online) Time-dependent average current at the left [blue (dark gray)] and right [green (light gray)] interface and in the middle of region C [red (gray)] for pumping through a device region which extends from $x=-6$ to $x=6$ a.u. A traveling wave $U(x,t)=U_1\sin(qx-\omega_0 t)$ with $U_1=0.5$ a.u., $\omega_0=0.8$ a.u., and $q=0.6$ a.u. is superimposed to the static potential $U_0(x)=U_C[1+\cos(kx)]$ with $U_C=0.5$ a.u. and $k=10\pi/6\sim5.2$ a.u., and the all system is unbiased, see inset. The straight line corresponds to the value of the average current as obtained from the Floquet algorithm which yields $I_{L,\mathrm{dc}}=-3.26\times10^{-2}$ a.u.

$U_1=0.5$ a.u., $\omega_0=0.8$ a.u., and $q=0.6$ a.u., we have found that the minimum current occurs at $\varepsilon_F=3.0$ a.u. All parameters in this example have been chosen to better illustrate and discuss the effect of the current inversion. The present section is not intended to give a realistic description of some specific experiment.

In Fig. 4, we plot the time-dependent average current [see Eq. (37)] in three different points of the device region. For the numerical propagation, we have used a lattice spacing $\Delta x=0.06$ a.u., a time step $2\delta=0.02$ a.u., and 400 k points between 0 and $k_F=\sqrt{2\varepsilon_F}$. The system responds to a right-moving traveling wave by generating a net current flowing to the left. Again, we observe that the transient time is of the order of few tens of a.u., and that the steady value is independent of the position. As in the previous example, we used the Floquet algorithm of the Appendix for benchmarking our real-time propagation algorithm. Due to the high Fermi energy, the calculation was carried out with $m_{\max}=15$ and $N_\omega=400$ energy points between 0 and ε_F. The result $I_{L,\mathrm{dc}}=-3.26\times10^{-2}$ a.u. is displayed in Fig. 4 with a straight line and is in extremely good agreement with the long-time limit of the average current obtained from direct propagation in time.

To understand how the electron fluid moves when the direction of the current is opposite to that of the driving potential wave, we have studied the dynamical flow pattern of the density. Such a study has the merit of providing a picture of the microscopic dynamics which is complementary to the ones of Floquet-based approaches (adiabatic picture, high frequency limit, theory of linear response, etc.), and hence helpful for a better qualitative understanding.

In Fig. 5, we display a contour plot of the excess density $\Delta\rho(x,t)=\rho(x,t)-\rho(x,0)$ in an extended region which includes the device region and a portion of the left reservoir. In the device region, we clearly see pockets that are dragged by

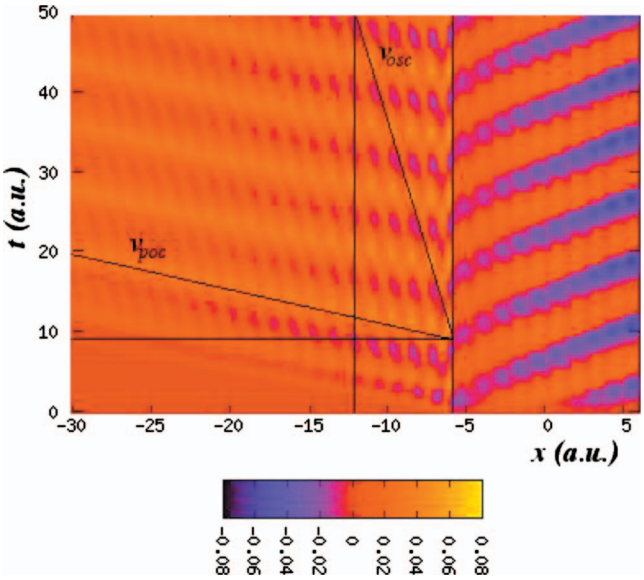

FIG. 5. (Color) Contour plot of the excess density $\Delta\rho(x,t)$ in the device region (x between −6 and 6 a.u.) and in a portion of the left reservoir (x between −30 and −6 a.u.). Due to the large oscillations of the excess density in the device region, $\Delta\rho(x,t)$ has been scaled down by a factor of 10 for $|x|<6$ a.u.. We also draw straight lines to show a pocket trajectory and the trajectory of a superimposed oscillation. All parameters are the same as for Fig. 4.

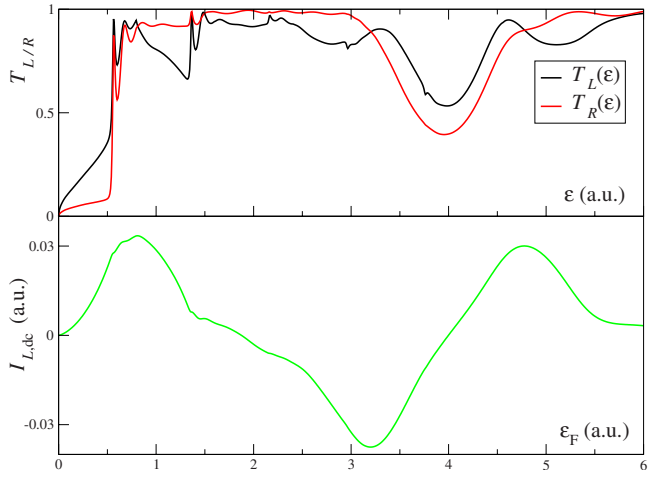

FIG. 6. (Color online) dc component of pump current $I_{L,\mathrm{dc}}$ and left (black) and right [red (gray)] transmission probabilities $T_{L/R}$ as function of the Fermi energy. The curves have been obtained using the Floquet algorithm of the Appendix with $m_{\max}=15$ and $N_\omega=800$ energy points between 0 and $\varepsilon_F=6$ a.u.

the traveling wave and are moving to the right. However, every pocket with a slightly positive $\Delta\rho$ is followed by a pocket with a noticeably negative $\Delta\rho$, and the net excess density is negative. On the other hand, in the left reservoir, pockets with negative $\Delta\rho$ are damped very fast away from the interface between device region and lead, while pockets with positive $\Delta\rho$ move to the left. We conclude that the driving produces right-moving "bubbles" in the device region and that to each bubble corresponds a more dense region of fluid moving to the left. One can estimate the speed v_{poc} of the traveling pockets from the slope of the patterns at constant density and finds $v_{\mathrm{poc}}\sim\omega_0/q\sim 1.33$ a.u., as expected. We also notice superimposed density oscillations on each pocket. These oscillations have the same spatial period of the static corrugation in the device region, and move in the same direction of the pockets at a constant speed $v_{\mathrm{osc}}\sim\omega_0/k\sim 0.15$ a.u.

In Fig. 6, we illustrate how the pumped current in this model depends on the Fermi level. For Fermi energies comparable to the amplitude of the corrugated potential in the device region, the pumping current is always positive, i.e., follows the propagation of the perturbed wave. However, there are striking effects that are more or less independent of the strength of the perturbation: the pumping current reaches a maximum positive value at $\varepsilon_F\sim\omega_0=0.8$ a.u., then decreases with increasing Fermi energy (with the turning point to negative values just below $\varepsilon_F=2$ a.u.) and reaches a minimum (negative) value above $\varepsilon_F=3$ a.u. To rationalize this behavior, we have calculated the total transmission probabilities $T_\alpha=\Sigma_m T_{m,\alpha}$, $\alpha=L,R$, for left- and right-going electrons [see Eqs. (11) and (12)]. As one can see from Fig. 6, both T_L and T_R remain quite small for Fermi energies below $\Delta\sim 0.54$ a.u., which roughly corresponds to the bottom of the lowest band of the periodic structure of the device. In this energy window, transport is dominated by tunneling and the pumping current follows the traveling wave ($T_L>T_R$) similar to the case of the Archimedean screw, see Sec. III A. For $\varepsilon_F>\Delta$, we enter the region of resonant transport (the energy of the lowest band) and T_L, T_R sharply increase. We observe that for $\varepsilon_F<\omega_0=0.8$ a.u., both T_L and T_R have a structure similar to the total transmission function of the static case. For $\omega_0<\varepsilon_F<\omega_0+\Delta$, however, T_L decreases significantly while T_R remains fairly constant around 1. We interpret this in the following way. The probability of the right-going electrons of emitting a photon of frequency ω_0 (and therefore reducing their energy) is larger than for the left-going electrons. Losing this energy, the transmission T_L resembles the static transmission function for energy $\varepsilon_F-\omega_0$, which has a much lower value. The asymmetry between left- and right-going states can be easily understood by realizing that the pump wave introduces a preferential direction in the problem. As further evidence to support this interpretation, we note that for $\varepsilon_F=\omega_0+\Delta$, the transmission function T_L increases rapidly as for $\varepsilon_F=\Delta$. This can be viewed as a replica of the static transmission function shifted by one quantum of energy ω_0. Throughout the energy window of the lowest band, T_L remains lower than T_R. As a consequence, the pumping current decreases monotonically. This behavior is reversed when the Fermi energy hits the top of the lowest band, around 3.4 a.u. In the gap (of about $2U_C=1$ a.u.), both T_L and T_R drop and transport is dominated by tunneling again. In this region, $T_L>T_R$ and the pumping current increases.

It is interesting to realize that despite the simplicity of the model, the pumped current has the same qualitative behavior as the pumped current measured by Leek *et al.*,[6] the only difference being a nonvanishing pumped current at Fermi energies comparable with the bottom of the band of the device. This difference is simply due to residual tunneling, an

effect which would drop off by making the central device larger. The present model gives positive and negative pumping currents as a function of the Fermi energy and provides a simple physical interpretation of the effect of current inversion. Our picture, however, is somewhat different from the one given in Ref. 6. Indeed, in their explanation, the sign of the pumping current is independent of the frequency ω_0 of the traveling wave. On the other hand, in our case, if the frequency exceeds the width of the lowest band, the right-going electrons cannot emit a photon and current inversion is not guaranteed anymore.

C. Transients effects

As a last example, we study electron pumping in quantum wells. We will show the presence of long-lived superimposed oscillations whose frequency is generally not commensurable with the driving frequency. The quantum well is modeled with a static potential $U_0(x)=-1.4$ a.u., for $|x|<1.2$ a.u. and zero otherwise. Initially, the system is in the ground state with Fermi energy $\varepsilon_F=0.1$ a.u. The unperturbed Hamiltonian has two bound-state eigensolutions with energies $\varepsilon^0_{b,1}=-1.035$ a.u. and $\varepsilon^0_{b,2}=-0.156$ a.u. The ground-state Slater determinant contains all extended states with energy between 0 and ε_F and two localized states with negative energy. At positive times, a constant bias $U_R=0.1$ a.u. is applied on the right lead and a traveling wave $U(x,t)=U_1\sin(qx-\omega_0 t)$, with $q=0.5$ a.u. and $\omega_0=0.5$ a.u., is switched on in the quantum well. In the numerical simulations, we set the propagation window between $x=-1.2$ and $x=1.2$ a.u. (which coincides with the static potential well) and choose a lattice spacing $\Delta x=0.024$ a.u. The occupied part of the continuum spectrum is discretized with 100 k points between 0 and $k_F=\sqrt{2\varepsilon_F}$.

Let us first consider the biased system with no driving, i.e., $U_1=0$. We propagate the (noninteracting) many-body state from $t=0$ to $t=1400$ a.u. using a time step $2\delta=0.05$ a.u., and calculate the current $I(t)$ at the center of the quantum well. As in the examples of Secs. III A and III B, one observes a first transient behavior which lasts for few tens of a.u. However, after this first normal transient, a second transient regime sets in. In Fig. 7, we plot the modulus of the discrete Fourier transform of the current

$$\tilde{I}(\omega_k)=2\delta\sum_{n=n_p}^{n_p+N_0} I(2n\delta)e^{-i\omega_k n\delta},\quad \omega_k=\frac{2\pi k}{N_0\delta} \tag{38}$$

for $n_p=(4+2p)\times 10^3$, $p=0,1,2,3,4$, and $N_0=16\times 10^3$ (corresponding to the time intervals $t\in(t_p,t_p+T_0)$ with $t_p=(2+p)\times 100$ a.u. and $T_0=800$ a.u. Besides the zero-frequency peak (not shown) due to the nonvanishing dc current, the structure of $\tilde{I}(\omega)$ has five more peaks. Below, we discuss the physical origin of these extra peaks and show that they are related to different kinds of internal transitions.

We first observe that the biased system has two bound states with energy $\varepsilon^\infty_{b,1}=-1.032$ a.u. and $\varepsilon^\infty_{b,2}=-0.133$ a.u. (slightly different from the bound-state energies of the unbiased system). The first and the last two peaks occur at the same frequency of the bound-continuum transitions $\varepsilon^\infty_{b,i}\to\varepsilon_F$, and $\varepsilon^\infty_{b,i}\to\varepsilon_F+U_R$, with $i=1,2$. These sharp structures (mathematically stemming from the discontinuity of the zero-temperature Fermi distribution function) give rise to long-lived oscillations of the total current and density. Such an oscillatory transient regime dies off slowly as $1/t$. The power-law behavior can also be seen in the inset of Fig. 7, where a magnification of the region with transitions from the weakly bound electron to the two continua is displayed. Denoting with R_p the product between the height of the second peak and the propagation time t_p+T_0, we have found $R_2=26.305$ a.u., $R_3=26.307$ a.u., and $R_4=26.328$ a.u., which is in fairly good agreement with the expected $1/t$ behavior. Therefore, the height of the peaks decreases with increasing t_p and approaches zero in the limit $t_p\to\infty$. On the contrary, the sharp peak at $\omega=\varepsilon^\infty_{b,1}-\varepsilon^\infty_{b,2}$ (bound-bound transition) remains unchanged with increasing t_p. The oscillations of the bound-bound transition do not die off, in agreement with the findings of Refs. 42 and 43. We emphasize that these latter have nothing to do with external drivings.

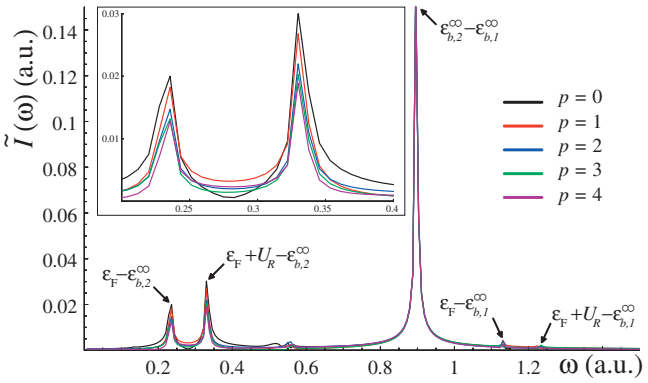

FIG. 7. (Color) Modulus of the discrete Fourier transform of the current for zero driving and $U_R=0.1$ a.u. The inset shows a magnification of the region with bound-continuum transitions. Different curves correspond to different time intervals.

Having discussed the behavior of the system which is biased but not driven, we now study transient regimes in the biased *and* driven system, i.e., $U_1\neq 0$. Using the same numerical parameters as in the previous example, we evolve the (noninteracting) many-body state from $t=0$ to $t=1200$ a.u., with a time step $2\delta=0.05$ a.u. In Fig. 8, we plot the discrete Fourier transform of the current calculated in the middle of the quantum well for different amplitudes of the traveling wave $U_1=0.00,0.01,0.03$ a.u. The time interval used to evaluate $\tilde{I}(\omega)$ is from $t=200$ a.u. to $t=1200$ a.u. As expected, $\tilde{I}(\omega)$ has a well pronounced peak at the driving frequency (first harmonic). Increasing the amplitude of the driving field, the height of the first-harmonic peak increases and higher-order harmonic peaks become visible (breakdown of linear response theory). This is clearly shown in inset (b) where the second-harmonic peak is visible for $U_1=0.03$ a.u. but not for $U_1=0.01$ a.u. The structure of $\tilde{I}(\omega)$ has also other peaks at frequencies which are not commensurable with the driving frequency. Such peaks are due to the presence of bound states in the biased-only system. In inset (a), we show a magnification of the region with bound-continuum transitions. The driving field broadens the peak

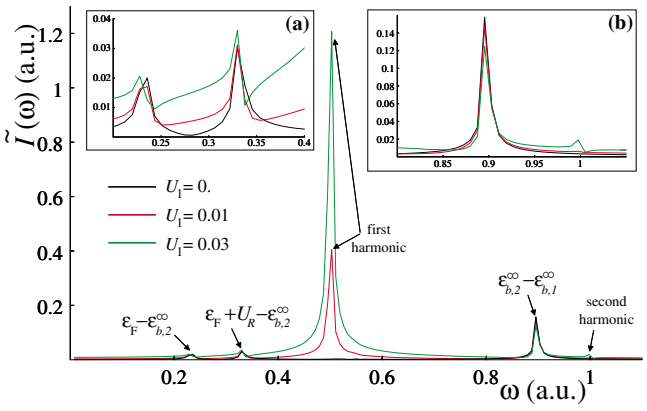

FIG. 8. (Color online) Modulus of the discrete Fourier transform of the current for the biased quantum well (U_R=0.1 a.u.) perturbed by the traveling wave $U(x,t)=U_1 \sin(qx-\omega t)$, with q=0.5 a.u. and ω=0.5 a.u. Three different amplitudes U_1=0.00 (black), 0.01 [red (gray)], and 0.03 [green (dark gray)] a.u. are considered. Inset (a) displays a magnification of the region with bound-continuum transitions. Inset (b) shows a magnification of the region with the bound-bound transition and the second-harmonic peak.

structure, thus speeding up the power-law transient regime. The shape of the bound-bound transition is displayed in inset (b). The height of the peak decreases with increasing amplitudes and the transition changes from an infinitely long-lived excitation to an excitation with a finite lifetime. Let m_s be the smallest integer for which $m_s\omega_0 > \max(|\varepsilon^{\infty}_{b,1}|, |\varepsilon^{\infty}_{b,2}|)$; for small amplitudes, the lifetime is proportional to $(1/U_1^2)^{m_s}$ according to the following reasoning. The retarded Green's function in region C can be written in terms of the embedding self-energy of Eq. (4) and the Floquet self-energy $\mathbf{\Sigma}^R_{\rm ac}$ of Eq. (A18). The Floquet self-energy generates replica of the continuous spectrum which are shifted by multiple integers of ω_0 and contributes to the imaginary part of the Green's function, $\mathbf{G}^R$. The leading-order contribution of the mth replica to $\mathrm{Im}\,\mathbf{G}^R$ scales like $(U_1^2)^m$. Therefore, bound-state simple poles of $\mathbf{G}^R$ get embedded in the continuum spectrum of some of the replica and acquire an imaginary part proportional to $(U_1^2)^m$, with m the order of the replica. The leading-order contribution to the life time of the bound-bound excitation is then proportional to $(1/U_1^2)^{m_s}$.

In conclusion, we have shown that the biased and driven quantum well has a very rich transient structure. This is due to the presence of bound states which can substantially delay the development of the Floquet regime.

IV. CONCLUSIONS AND OUTLOOK

Time-dependent gate voltages can be used to generate a net current between unbiased electrodes in nanoscale junctions. Most works focus on periodic drivings for which Floquet-based approaches provide a powerful machinery to investigate the long-time behavior of the system. Combining Floquet theory with nonequilibrium Green's functions techniques, we obtained a general formula for the average current of monochromatically driven systems in terms of inelastic transmission probabilities. The case of polychromatic drivings, which has received scarce attention so far, is analytically more complicated and computationally rather costly.

In this work, we proposed an alternative approach which can deal with monochromatic, polychromatic, and nonperiodic drivings. The computational cost is independent of the particular time dependence of the driving potential. As an extra bonus, we can investigate how the transient behavior depends on the initial state and on the details of the switching process. The basic idea is to calculate the time-dependent density and current from the time-evolved (noninteracting) many-particle state. This amounts to solving a single-particle Schrödinger equation for each occupied eigenstate of the unperturbed system. We have given full implementation details of the time-propagation algorithm and discussed its performance. The generalization to two-or three-dimensional reservoirs can be worked out following the general lines of Ref. 19 and its implementation is in progress.

We illustrated our scheme in one-dimensional structures. First, we studied pumping through a single barrier, and showed that the electrons are dragged by the traveling wave and move in pockets. Second, we studied pumping in semiconducting structures, and investigated the phenomenon of current inversion. In both examples, the Floquet algorithm of the Appendix is used for benchmarking the long-time limit of the real-time simulations and we have found an excellent agreement between the two approaches. Finally, we considered pumping through a quantum well connected to biased reservoirs. The aim of this latter example is to show the existence of a long-lived transient regime in rather common physical systems. The transient oscillations are explained in terms of bound-bound transitions and bound-continuum transitions. These oscillations usually have frequencies which are not commensurable with the driving frequency and are therefore not described by the initial Floquet assumption. In fact, we believe that this is a rather important result. It implies that the basic assumption behind the Landauer-Büttiker approach that a steady state is reached in the long-time limit is generally not true.

The present work opens the path toward systematic studies of nanoscale devices as it is not restricted to linear response theory and can cope with general time-dependent as well as spatial perturbations. Our approach can also be extended in a natural way to describe more complicated physical systems. The effects of electron correlation may be included within the framework of time-dependent density functional theory[19] by using present exchange-correlation density functionals as well as orbital dependent ones. Second, the scheme can be upgraded to cope with three-dimensional reservoirs. This is computationally more demanding but clearly will pay back in our understanding of nonequilibrium dynamical phenomena in nanoconstrictions.

Highlighting different physical phenomena, our idea of real-time evolution of open quantum systems may also be used to address questions such as time-dependent spin transport, current fluctuations and shot noise, optimal control of devices for quantum information processing,[49] the role of superconducting leads, heat transport, etc. In particular, the design of fast, integrated, optoelectronic nanodevices clearly requires the proper description of dynamical effects (relaxation, decoherence, etc.) on a microscopic level. Problems

related to current induced heating and electromigration should also be addressed,[23,50–52] and one might need to go beyond the classical treatment of the ionic motion as it fails in describing Joule heating.[53–55] The present work is a small step toward those ambitious goals, adding the physics of time-dependent phenomena to the world of steady-state effects in quantum transport.

ACKNOWLEDGMENTS

We thank E. Khosravi, C. Verdozzi, and H. Appel for useful discussions. This work was supported in part by the Deutsche Forschungsgemeinschaft, DFG programme SFB658, the EU Network of Excellence NANOQUANTA (NMP4-CT-2004-500198), the SANES project (NMP4-CT-2006-017310), the DNA-NANODEVICES (IST-2006-029192), the 2005 Bessel research support of the Humboldt Foundation, and the BSC (Barcelona Mare Nostrum Center).

APPENDIX: CURRENT FORMULA

The dc kernel $\mathbf{Q}_{\alpha,\mathrm{dc}}$ in Eq. (7) is given by the sum of two terms, both containing an integral over energy ω. Consequently, also the total dc current can be expressed as the sum of two terms. From Eq. (2), it is straightforward to obtain

$$I_{\alpha,\mathrm{dc}} = I_\alpha^{(1)} + I_\alpha^{(2)}, \tag{A1}$$

with

$$I_\alpha^{(1)} = -2\int \frac{d\omega}{2\pi} f_\alpha(\omega)\,\mathrm{Im}\,\mathrm{Tr}[\mathbf{\Gamma}_\alpha(\omega)\mathbf{G}_0(\omega)], \tag{A2}$$

and

$$I_\alpha^{(2)} = -\int \frac{d\omega}{2\pi}\sum_\beta f_\beta(\omega) \times \sum_m \mathrm{Tr}[\mathbf{G}_m(\omega)\mathbf{\Gamma}_\beta(\omega)\mathbf{G}_m^\dagger(\omega)\mathbf{\Gamma}_\alpha(\omega - m\omega_0)]. \tag{A3}$$

Below we use the recursive scheme by Martinez[39] to calculate the coefficients $\mathbf{G}_m$. We write the Hamiltonian $\mathbf{H}_{CC}(t)$ as the sum of a static, $\mathbf{H}_{CC}^0$, and periodic, $\mathbf{U}_{CC}(t)$, term and expand the latter in Fourier modes

$$\mathbf{U}_{CC}(t) = \sum_n \mathbf{U}_n e^{in\omega_0 t}, \quad \mathbf{U}_n = \mathbf{U}_{-n}^\dagger. \tag{A4}$$

We also define the Green's function $\mathbf{g}$ as the projection onto region C of the Green's function of the system which is biased but not driven, i.e., $\mathbf{U}_{CC}(t)=0$. The Green's function $\mathbf{g}$ depends only on the difference between its time arguments and can be expanded as follows:

$$\mathbf{g}^R(t;t') = \sum_m \int \frac{d\omega}{2\pi}\mathbf{g}_m^R(\omega)e^{-i\omega(t-t')+im\omega_0 t'}, \tag{A5}$$

where the only nonvanishing coefficient of the expansion is $\mathbf{g}_0^R(\omega)$ and reads

$$\mathbf{g}_0^R(\omega) = 1/[\omega\mathbf{1}_C - \mathbf{H}_{CC}^0 - \mathbf{\Sigma}^R(\omega)], \tag{A6}$$

with $\mathbf{1}_C$ the unit matrix in region C and $\mathbf{\Sigma}^R$ the retarded embedding self-energy of Eq. (4). Inserting the above expansions into the Dyson equation

$$\mathbf{G}^R(t;t') = \mathbf{g}^R(t;t') + \int d\bar{t}\mathbf{g}^R(t;\bar{t})\mathbf{U}_{CC}(\bar{t})\mathbf{G}^R(\bar{t};t'), \tag{A7}$$

we find a set of linear equations for the coefficients $\mathbf{G}_m$

$$\mathbf{G}_m(\omega) = \delta_{m,0}\mathbf{g}_m(\omega) + \mathbf{g}_m(\omega)\sum_n \mathbf{U}_n\mathbf{G}_{m-n}(\omega), \tag{A8}$$

where we have used the short-hand notation $\mathbf{g}_m(\omega)=\mathbf{g}_0^R(\omega - m\omega_0)$ [the $\mathbf{g}_m$ should not to be confused with the expansion coefficient $\mathbf{g}_m^R$ of Eq. (A5); the latter is zero for all $m\neq 0$]. For arbitrary periodic drivings, the solution of Eq. (A8) is computationally very hard. In the following, we specialize to the monochromatic case and describe a feasible numerical scheme to calculate the $\mathbf{G}_m$'s.

For monochromatic drivings, $\mathbf{U}_n=\delta_{n,1}\mathbf{U}_+ + \delta_{n,-1}\mathbf{U}_-$, the algebraic system in Eq. (A8) simplifies to (understanding the quantities as function of ω)

$$\mathbf{G}_m = \mathbf{g}_m[\delta_{m,0} + \mathbf{U}_+\mathbf{G}_{m-1} + \mathbf{U}_-\mathbf{G}_{m+1}], \tag{A9}$$

which is a tridiagonal system. In matrix form Eq. (A9) reads

$$\left[\begin{array}{ccc|c|ccc} & & & \vdots & & & \\ & \underline{\mathbf{M}}^{(-)} & & 0 & & \underline{\mathbf{0}} & \\ & & & 0 & & & \\ & & & -\mathbf{g}_{-1}\mathbf{U}_- & & & \\ \hline \cdots\ 0 & 0 & -\mathbf{g}_0\mathbf{U}_+ & \mathbf{1}_C & -\mathbf{g}_0\mathbf{U}_- & 0 & 0\ \cdots \\ \hline & & & -\mathbf{g}_1\mathbf{U}_+ & & & \\ & & & 0 & & & \\ & \underline{\mathbf{0}} & & 0 & & \underline{\mathbf{M}}^{(+)} & \\ & & & \vdots & & & \end{array}\right] \left[\begin{array}{c} \vdots \\ \mathbf{G}_{-3} \\ \mathbf{G}_{-2} \\ \mathbf{G}_{-1} \\ \hline \mathbf{G}_0 \\ \hline \mathbf{G}_1 \\ \mathbf{G}_2 \\ \mathbf{G}_3 \\ \vdots \end{array}\right] = \left[\begin{array}{c} \vdots \\ 0 \\ 0 \\ 0 \\ \hline \mathbf{g}_0 \\ 0 \\ 0 \\ 0 \\ \vdots \end{array}\right] \tag{A10}$$

where $\underline{\mathbf{0}}$ is the null matrix and the matrices $\underline{\mathbf{M}}^{(\pm)}$ read

$$\underline{\mathbf{M}}^{(-)} = \begin{bmatrix} & \ddots & \ddots & 0 & 0 \\ \cdots & -\mathbf{g}_{-3}\mathbf{U}_+ & \mathbf{1}_C & -\mathbf{g}_{-3}\mathbf{U}_- & 0 \\ \cdots & 0 & -\mathbf{g}_{-2}\mathbf{U}_+ & \mathbf{1}_C & -\mathbf{g}_{-2}\mathbf{U}_- \\ \cdots & 0 & 0 & -\mathbf{g}_{-1}\mathbf{U}_+ & \mathbf{1}_C \end{bmatrix}, \tag{A11}$$

$$\underline{\mathbf{M}}^{(+)} = \begin{bmatrix} \mathbf{1}_C & -\mathbf{g}_1\mathbf{U}_- & 0 & 0 & \cdots \\ -\mathbf{g}_2\mathbf{U}_+ & \mathbf{1}_C & -\mathbf{g}_2\mathbf{U}_- & 0 & \cdots \\ 0 & -\mathbf{g}_3\mathbf{U}_+ & \mathbf{1}_C & -\mathbf{g}_3\mathbf{U}_- & \cdots \\ 0 & 0 & \ddots & \ddots & \end{bmatrix}. \tag{A12}$$

Let $\mathbf{M}_-^{-1}$, $\mathbf{M}_+^{-1}$ be the bottom-right block of the inverse of $\underline{\mathbf{M}}^{(-)}$ and the top-left block of the inverse of $\underline{\mathbf{M}}^{(+)}$, respectively. The coefficient $\mathbf{G}_{\pm 1}$ can be expressed in terms of $\mathbf{M}_\pm^{-1}$ according to

$$\mathbf{G}_{\pm 1} = \mathbf{M}_\pm^{-1}\mathbf{g}_{\pm 1}\mathbf{U}_\pm\mathbf{G}_0. \tag{A13}$$

Substituting this result into Eq. (A9) with $m=0$, one obtains a closed equation for $\mathbf{G}_0$

$$\mathbf{G}_0 = \mathbf{g}_0 + \mathbf{g}_0 \sum_\pm \mathbf{U}_\mp \mathbf{M}_\pm^{-1}\mathbf{g}_{\pm 1}\mathbf{U}_\pm\mathbf{G}_0. \tag{A14}$$

Exploiting the tridiagonal block structure of $\underline{\mathbf{M}}^{(\pm)}$, we can express the matrices $\mathbf{M}_\pm^{-1}$ as a continued matrix fraction

$$\mathbf{M}_\pm^{-1} = \cfrac{\mathbf{1}_C}{\mathbf{1}_C - \mathbf{g}_{\pm 1}\mathbf{U}_\mp \cfrac{\mathbf{1}_C}{\mathbf{1}_C - \mathbf{g}_{\pm 2}\mathbf{U}_\mp \cfrac{\mathbf{1}_C}{\ddots}\mathbf{g}_{\pm 3}\mathbf{U}_\pm}\mathbf{g}_{\pm 2}\mathbf{U}_\pm} = \cfrac{\mathbf{1}_C}{\mathbf{g}_{\pm 1}^{-1} - \mathbf{U}_\mp \cfrac{\mathbf{1}_C}{\mathbf{g}_{\pm 2}^{-1} - \mathbf{U}_\mp \cfrac{\mathbf{1}_C}{\ddots}\mathbf{U}_\pm}\mathbf{U}_\pm}\mathbf{g}_{\pm 1}^{-1}, \tag{A15}$$

which is equivalent to solving the following recursive relations (remaking explicit the dependence on ω):

$$\mathbf{M}_\pm^{-1}(\omega) = \mathbf{H}_{\pm,1}^{-1}(\omega)\mathbf{g}_{\pm 1}^{-1}(\omega). \tag{A16}$$

and

$$\mathbf{H}_{\pm,m}^{-1}(\omega) = \frac{\mathbf{1}_C}{\mathbf{g}_{\pm m}^{-1}(\omega) - \mathbf{U}_\mp\mathbf{H}_{\pm,m+1}^{-1}(\omega)\mathbf{U}_\pm} = \frac{\mathbf{1}_C}{(\omega \mp m\omega_0)\mathbf{1}_C - \mathbf{H}_{CC}^0 - \boldsymbol{\Sigma}^R(\omega \mp m\omega_0) - \mathbf{U}_\mp\mathbf{H}_{\pm,m+1}^{-1}(\omega)\mathbf{U}_\pm}. \tag{A17}$$

Introducing the ac self-energy,

$$\boldsymbol{\Sigma}_{\mathrm{ac}}^R(\omega) = \sum_\pm \mathbf{U}_\mp\mathbf{H}_{\pm,1}^{-1}(\omega)\mathbf{U}_\pm, \tag{A18}$$

which accounts for the interaction between the electrons and the ac driving field, we can rewrite the solution for $\mathbf{G}_0$ in Eq. (A14) as

$$\mathbf{G}_0^{-1}(\omega) = \mathbf{g}_0^{-1}(\omega) - \boldsymbol{\Sigma}_{\mathrm{ac}}^R(\omega) = \omega\mathbf{1}_C - \mathbf{H}_{CC}^0 - \boldsymbol{\Sigma}^R(\omega) - \boldsymbol{\Sigma}_{\mathrm{ac}}^R(\omega). \tag{A19}$$

In our implementation, we have solved the above recursive relations by truncating the hierarchy. For some $m = m_{\max}$, we set $\mathbf{H}_{\pm,m_{\max}}(\omega) = \mathbf{g}_{\pm m_{\max}}^{-1}(\omega)$, and calculate all the $\mathbf{H}_{\pm,m}(\omega)$ with $m < m_{\max}$ according to Eq. (A17). The convergence of the result can be tested by increasing $m_{\max}$. Typically, the smaller ω_0 the larger one has to choose $m_{\max}$ to achieve convergence. Once the matrix $\mathbf{G}_0$ has been calculated, the matrices $\mathbf{G}_m$ with $m \neq 0$ are easily obtained from

$$\mathbf{G}_{\pm m}(\omega) = \mathbf{H}_{\pm,m}^{-1}(\omega)\mathbf{U}_\pm\mathbf{G}_{\pm(m-1)}(\omega), \quad m > 0. \tag{A20}$$

Having explicit equations for the $\mathbf{G}_m$'s, we now show how to express the total dc current in terms of inelastic transmission probabilities. To calculate the contribution $I_\alpha^{(1)}$ in Eq. (A2), we need to evaluate the imaginary part of $\mathrm{Tr}[\boldsymbol{\Gamma}_\alpha\mathbf{G}_0]$. Using the identity

$$\mathbf{G}_0 - \mathbf{G}_0^\dagger = \mathbf{G}_0^\dagger(\boldsymbol{\Sigma}^R - [\boldsymbol{\Sigma}^R]^\dagger + \boldsymbol{\Sigma}_{\mathrm{ac}}^R - [\boldsymbol{\Sigma}_{\mathrm{ac}}^R]^\dagger)\mathbf{G}_0, \tag{A21}$$

we find

$$\mathrm{Im}\,\mathrm{Tr}[\boldsymbol{\Gamma}_\alpha\mathbf{G}_0] = \frac{1}{2i}\mathrm{Tr}[\boldsymbol{\Gamma}_\alpha(\mathbf{G}_0 - \mathbf{G}_0^\dagger)] = -\frac{1}{2}\mathrm{Tr}[\boldsymbol{\Gamma}_\alpha\mathbf{G}_0^\dagger(\boldsymbol{\Gamma} + \boldsymbol{\Gamma}_{\mathrm{ac}})\mathbf{G}_0], \tag{A22}$$

where we have defined $\boldsymbol{\Gamma} = \boldsymbol{\Gamma}_L + \boldsymbol{\Gamma}_R = i(\boldsymbol{\Sigma}^R - [\boldsymbol{\Sigma}^R]^\dagger)$ and $\boldsymbol{\Gamma}_{\mathrm{ac}} = i(\boldsymbol{\Sigma}_{\mathrm{ac}}^R - [\boldsymbol{\Sigma}_{\mathrm{ac}}^R]^\dagger)$. From the recursive relation (A20) and the definition of $\boldsymbol{\Sigma}_{\mathrm{ac}}^R$ in Eq. (A18), we have

$$\mathbf{G}_0^\dagger\boldsymbol{\Sigma}_{\mathrm{ac}}^R\mathbf{G}_0 = \sum_\pm \mathbf{G}_0^\dagger\mathbf{U}_\mp\mathbf{H}_{\pm,1}^{-1}\mathbf{U}_\pm\mathbf{G}_0 = \sum_\pm \mathbf{G}_{\pm 1}^\dagger\mathbf{H}_{\pm,1}^\dagger\mathbf{G}_{\pm 1}, \tag{A23}$$

and hence

$$\mathbf{G}_0^\dagger\boldsymbol{\Gamma}_{\mathrm{ac}}\mathbf{G}_0 = i\sum_\pm \mathbf{G}_{\pm 1}^\dagger(\mathbf{H}_{\pm,1}^\dagger - \mathbf{H}_{\pm,1})\mathbf{G}_{\pm 1}. \tag{A24}$$

Next, we use the recursive relations (A17) and find

$$\mathbf{H}^{\dagger}_{\pm,1}(\omega) - \mathbf{H}_{\pm,1}(\omega) = -i\mathbf{\Gamma}(\omega \mp \omega_0) + \mathbf{U}_{\mp}(\mathbf{H}^{-1}_{\pm,2}(\omega) - [\mathbf{H}^{-1}_{\pm,2}(\omega)]^{\dagger})\mathbf{U}_{\pm}. \quad \text{(A25)}$$

Inserting this result into Eq. (A24) yields

$$\mathbf{G}^{\dagger}_0(\omega)\mathbf{\Gamma}_{\rm ac}(\omega)\mathbf{G}_0(\omega) = \sum_{\pm} \mathbf{G}^{\dagger}_{\pm 1}(\omega)\mathbf{\Gamma}(\omega \mp \omega_0)\mathbf{G}_{\pm 1}(\omega) + i\sum_{\pm} \mathbf{G}^{\dagger}_{\pm 1}(\omega)\mathbf{U}_{\mp}([\mathbf{H}^{-1}_{\pm,2}(\omega)]^{\dagger} - \mathbf{H}^{-1}_{\pm,2}(\omega))\mathbf{U}_{\pm}\mathbf{G}_{\pm 1}(\omega). \quad \text{(A26)}$$

The second term on the r.h.s. can be expressed in terms of $\mathbf{G}_{\pm 2}$ with the help of Eq. (A20). In doing so, we obtain a first term given by $\Sigma_{\pm}\mathbf{G}^{\dagger}_{\pm 2}(\omega)\mathbf{\Gamma}(\omega \mp 2\omega_0)\mathbf{G}_{\pm 2}(\omega)$, and a second term that can be expressed in terms of $\mathbf{G}_{\pm 3}$. Iterating *ad infinitum*, we end up with the following expression:

$$\mathbf{G}^{\dagger}_0(\omega)\mathbf{\Gamma}_{\rm ac}(\omega)\mathbf{G}_0(\omega) = \sum_{m>0}\sum_{\pm} \mathbf{G}^{\dagger}_{\pm m}(\omega)\mathbf{\Gamma}(\omega \mp m\omega_0)\mathbf{G}_{\pm m}(\omega), \quad \text{(A27)}$$

and therefore

$$\mathrm{Im\,Tr}[\mathbf{\Gamma}_{\alpha}(\omega)\mathbf{G}_0(\omega)] = -\frac{1}{2}\sum_{m} \mathrm{Tr}[\mathbf{\Gamma}_{\alpha}(\omega)\mathbf{G}^{\dagger}_m(\omega)\mathbf{\Gamma}(\omega - m\omega_0)\mathbf{G}_m(\omega)]. \quad \text{(A28)}$$

Substituting this result back into Eq. (A2) and performing the sum $I^{(1)}_{\alpha} + I^{(2)}_{\alpha}$, with $I^{(2)}_{\alpha}$ from Eq. (A3), we obtain the total dc in terms of inelastic transmission probabilities [see Eq. (10)]. The above derivation is based on nonequilibrium Green's functions, and generalizes a previous derivation[17] to central regions of dimension larger than one.

*gianluca@physik.fu-berlin.de

[1] A collection of recent articles on this field can be found in *Molecular Electronics*, edited by G. Cuniberti, G. Fagas, and K. Richter (Springer, Berlin, 2005).
[2] D. J. Thouless, Phys. Rev. B **27**, 6083 (1983).
[3] C. A. Stafford and N. S. Wingreen, Phys. Rev. Lett. **76**, 1916 (1996).
[4] P. W. Brouwer, Phys. Rev. B **58**, R10135 (1998).
[5] M. Switkes, C. M. Marcus, K. Campman, and A. C. Gossard, Science **283**, 1905 (1999).
[6] P. J. Leek, M. R. Buitelaar, V. I. Talyanskii, C. G. Smith, D. Anderson, G. A. C. Jones, J. Wei, and D. H. Cobden, Phys. Rev. Lett. **95**, 256802 (2005).
[7] L. DiCarlo, C. M. Marcus, and J. S. Harris, Jr., Phys. Rev. Lett. **91**, 246804 (2003).
[8] M. G. Vavilov, L. DiCarlo, and C. M. Marcus, Phys. Rev. B **71**, 241309(R) (2005).
[9] B. Wang, J. Wang, and H. Guo, Phys. Rev. B **65**, 073306 (2002).
[10] L. E. F. Foa Torres, Phys. Rev. B **72**, 245339 (2005).
[11] The variation in time has to be much longer than the dwelling time for an electron in the device.
[12] B. L. Altshuler and L. I. Glazman, Science **283**, 1864 (1999).
[13] M. Büttiker, H. Thomas, and A. Pretre, Z. Phys. B: Condens. Matter **94**, 133 (1994).
[14] M. Büttiker and M. Moskalets, Lect. Notes Phys. **690**, 33 (2006).
[15] F. Zhou, B. Spivak, and B. Altshuler, Phys. Rev. Lett. **82**, 608 (1999).
[16] S. Camalet, J. Lehmann, S. Kohler, and P. Hänggi, Phys. Rev. Lett. **90**, 210602 (2003).
[17] L. Arrachea, Phys. Rev. B **72**, 125349 (2005).
[18] L. Arrachea and M. Moskalets, Phys. Rev. B **74**, 245322 (2006).
[19] S. Kurth, G. Stefanucci, C.-O. Almbladh, A. Rubio, and E. K. U. Gross, Phys. Rev. B **72**, 035308 (2005).
[20] R. D'Agosta and M. Di Ventra, J. Phys.: Condens. Matter **18**, 11059 (2006).
[21] G. Stefanucci and C.-O. Almbladh, Phys. Rev. B **69**, 195318 (2004).
[22] V. Spicka, B. Velický, and A. Kalvová, Physica E (Amsterdam) **29**, 196 (2005).
[23] C. Verdozzi, G. Stefanucci, and C.-O. Almbladh, Phys. Rev. Lett. **97**, 046603 (2006).
[24] C. G. Sánchez, M. Stamenova, S. Sanvito, D. R. Bowler, A. P. Horsfield, and T. N. Todorov, J. Chem. Phys. **124**, 214708 (2006).
[25] J. Maciejko, J. Wang, and H. Guo, Phys. Rev. B **74**, 085324 (2006).
[26] N. Bushong, N. Sai, and M. Di Ventra, Nano Lett. **5**, 2569 (2005).
[27] D. Hou, Y. He, X. Liu, J. Kang, J. Chen, and R. Han, Physica E (Amsterdam) **31**, 191 (2006).
[28] H. Ishii, Y. Tomita, and T. Nakayama, Phys. Status Solidi C **4**, 481 (2007).
[29] N. Sai, N. Bushong, R. Hatcher, and M. Di Ventra, Phys. Rev. B **75**, 115410 (2007).
[30] V. Moldoveanu, V. Gudmundsson, and A. Manolescu, Phys. Rev. B **76**, 085330 (2007); **76**, 165308 (2007).
[31] H. Appel, S. Kurth, G. Stefanucci, A. Rubio, and E. K. U. Gross (unpublished).
[32] C. Caroli, R. Combescot, P. Nozìeres, and D. Saint-James, J. Phys. C **4**, 916 (1971).
[33] M. Cini, Phys. Rev. B **22**, 5887 (1980).
[34] G. Stefanucci and C.-O. Almbladh, Europhys. Lett. **67**, 14 (2004).
[35] A.-P. Jauho, N. S. Wingreen, and Y. Meir, Phys. Rev. B **50**, 5528 (1994).
[36] D. W. Hone, R. Ketzmerick, and W. Kohn, Phys. Rev. A **56**, 4045 (1997).
[37] Y. Meir and N. S. Wingreen, Phys. Rev. Lett. **68**, 2512 (1992).
[38] D. S. Fisher and P. A. Lee, Phys. Rev. B **23**, 6851 (1981).
[39] D. F. Martinez, J. Phys. A **36**, 9827 (2003).
[40] For a recent review, see S. Kohler, J. Lehmann, and P. Hänggi, Phys. Rep. **406**, 379 (2005), and references therein.
[41] See, for instance, X. Oriols, A. Alarcón, and E. Fernàndez-Díaz, Phys. Rev. B **71**, 245322 (2005), and references therein.

[42] A. Dhar and D. Sen, Phys. Rev. B **73**, 085119 (2006).
[43] G. Stefanucci, Phys. Rev. B **75**, 195115 (2007).
[44] We wish to observe that finite systems can be accurately described by finite matrices $\boldsymbol{H}(t)$, and the numerical integration of the Schrödinger equation becomes feasible for not too large sizes. The direct integration of the equations of motion has been recently used to study quantum pumps connected to *finite* electrodes. See A. Agarwal and D. Sen, J. Phys.: Condens. Matter **19**, 046205 (2007). One of the main merits of our algorithm is that it can deal with *infinitely* long electrodes since the transparent boundary conditions are implemented in an exact way.
[45] J. R. Hellums and W. R. Frensley, Phys. Rev. B **49**, 2904 (1994).
[46] E. Runge and E. K. U. Gross, Phys. Rev. Lett. **52**, 997 (1984).
[47] R. van Leeuwen, Phys. Rev. Lett. **82**, 3863 (1999).
[48] V. I. Talyanskii, D. S. Novikov, B. D. Simons, and L. S. Levitov, Phys. Rev. Lett. **87**, 276802 (2001).
[49] A step in this direction was done by E. Räsänen, A. Castro, J. Werschnik, A. Rubio, and E. K. U. Gross, Phys. Rev. Lett. **98**, 157404 (2007), where it has been shown that a full control of the current in a quantum ring can be achieved (qubit) using short shaped-laser pulses combining optimal-control theory and time-propagation schemes.
[50] M. Di Ventra and S. T. Pantelides, Phys. Rev. B **61**, 16207 (2000).
[51] A. P. Horsfield, D. R. Bowler, and A. J. Fisher, J. Phys.: Condens. Matter **16**, L65 (2004).
[52] Y. Miyamoto, A. Rubio, and D. Tomànek, Phys. Rev. Lett. **97**, 126104 (2006).
[53] A. P. Horsfield, D. R. Bowler, A. J. Fisher, T. N. Todorov, and M. J. Montgomery, J. Phys.: Condens. Matter **16**, 3609 (2004).
[54] A. P. Horsfield, D. R. Bowler, A. J. Fisher, T. N. Todorov, and C. G. Sanchez, J. Phys.: Condens. Matter **16**, 8251 (2004).
[55] D. R. Bowler, A. P. Horsfield, C. G. Sanchez, and T. N. Todorov, J. Phys.: Condens. Matter **17**, 3985 (2005).